Hindawi
Advances in Meteorology
Volume 2018, Article ID 2650642, 15 pages
https://doi.org/10.1155/2018/2650642

Research Article

The Impact of Façade Orientation and Woody Vegetation on Summertime Heat Stress Patterns in a Central European Square: Comparison of Radiation Measurements and Simulations

Noémi Kántor,[1] Csilla Viktória Gál,[2] Ágnes Gulyás,[1] and János Unger[1]

[1]*Department of Climatology and Landscape Ecology, University of Szeged, Egyetem u. 2, 6722 Szeged, Hungary*
[2]*School of Technology and Business Studies, Dalarna University, 79188 Falun, Sweden*

Correspondence should be addressed to János Unger; unger@geo.u-szeged.hu

Received 11 September 2017; Accepted 12 November 2017; Published 15 January 2018

Academic Editor: Hiroshi Tanaka

Increasing summertime air temperature deteriorates human health especially in cities where the warming tendency is exacerbated by urban heat island. Human-biometeorological studies shed light on the primary role of radiation conditions in the development of summertime heat stress. However, only a limited number of field investigations have been conducted up to now. Based on a 26-hour long complex radiation measurement, this study presents the evolved differences within a medium-sized rectangular square in Szeged, Hungary. Besides assessing the impact of woody vegetation and façade orientation on the radiation heat load, different modeling software programs (ENVI-met, SOLWEIG, and RayMan) are evaluated in reproducing mean radiant temperature (T_{mrt}). Although daytime T_{mrt} can reach an extreme level at exposed locations (65–75°C), mature shade trees can reduce it to 30–35°C. Nevertheless, shading from buildings adjacent to sidewalks plays also an important role in mitigating pedestrian heat stress. Sidewalks facing SE, S, and SW do not benefit from the shading effect of buildings; therefore, shading them by trees or artificial shading devices is of high importance. The measurement–model comparison revealed smaller or larger discrepancies that raise awareness of the careful adaptation of any modeling software and of the relevance of fine-resolution field measurements.

1. Introduction

Regional climate change is expected to bring rising air temperature values and to increase the frequency, length, and severity of heat waves in Central Europe, and thus in Hungary too [1, 2]. Combined with the peculiar climate of cities, characterized by increased air temperature and reduced ventilation due to the great amount of artificial materials, low vegetation rate, and the complex surface morphology [3], extreme heat events are expected to have more serious impacts on urban environments [4]. Without adaptation to heat waves people shall face deteriorating thermal comfort conditions, which in turn lead to declining working efficiency [5]. Moreover, intensification of heat stress is expected to increase the mortality rates, especially among the vulnerable groups, like infants, elderly people, and those with cardiovascular diseases [6]. In this respect it is worth emphasizing that, among the continents, Europe has the greatest percentage (24%) of its population aging 60 or over [7]. Furthermore, 73% of the European population already lives in urban areas, and by 2050 this proportion is expected to rise over 80% [7]. In the light of the mentioned warming, aging, and urbanization tendencies, mitigating the impact of extreme heat events should be one of the most important issues in urban planning [8–10].

Researchers in the field of urban human-biometeorology demonstrated that radiation heat load, quantified usually as mean radiant temperature (T_{mrt}) [[11–13] and see Section 2.2], is the main factor of daytime heat stress in summer in midlatitudes, and therefore shading, that is, the reduction of T_{mrt} is the most effective mean of heat stress mitigation in outdoor urban spaces [14–18]. Field measurements and simulation studies conducted at various climate zones (continental, arid, and tropical) have shown that larger tree canopy coverage and higher street aspect ratio (that is, shading by buildings) are generally the most effective design strategies

against urban heat stress [19–27]. Studies from cities with temperate climates commonly found that shading delivers the greatest human-biometeorological improvement [28–34]. It must be emphasized that only a limited number of field experiments have been conducted relying on the most accurate six-directional radiation measurement technique up to now, because this technique requires expensive and heavy instrumentation [[11–13] and see Section 2.2].

Numerical models are popular and easily obtainable alternatives of the time- and resource-consuming onsite investigations to determine T_{mrt}. For this purpose commonly used simulation software programs are ENVI-met [35–39], RayMan Pro [40–42], and SOLWEIG [43–46]. Although the number of simulation studies expands rapidly, only few of the modeled results have been validated with accurate onsite measurement. Except [47] that investigated several techniques in their capabilities to obtain T_{mrt}, the available validation studies focused usually only on one of the mentioned models, although comparison of their performance among different conditions, revealing their benefits and shortcomings, would be of great interest for professional urban planners and landscape designers. Experimental T_{mrt} values were used to validate ENVI-met in Freiburg, Germany [30, 37, 38], while the performance of RayMan was tested in various cities, that is, in Göteborg, Sweden [12], in Freiburg, Germany [40–42], in Glasgow, UK [48], and even in Huwei, Taiwan [22, 49]. The latter three validation studies relied on field surveys utilizing globe thermometers, although this technique has been demonstrated to be inappropriate in outdoor conditions [50]. In contrast, there are other studies where the model-measurement comparisons were based on the most accurate six-directional radiation measurement technique (e.g., [12, 30, 37, 38, 42, 47]). The low number of such validation studies can be explained by the expensive sensors, and the time and human-resource intensive nature of these measurements.

According to the above mentioned, this study intends to contribute to the urban human-biometeorological knowledge by conducting a detailed analysis of the evolved radiation conditions (radiation flux densities from six main directions) and the resulted T_{mrt} differences within a medium-sized rectangular square in Szeged, one of the warmest cities of Hungary. Special emphasis is put on the importance of sidewalks' exposure to direct irradiation, that is, the façade orientation of the buildings bordering the square and the role of woody vegetation in mitigating heat stress. Beside assessing the impact of shade trees and different façade orientations on the radiation heat load in a complex urban setting, this study aims to evaluate and compare ENVI-met, SOLWEIG, and RayMan in their ability to reproduce T_{mrt}.

2. Materials and Methods

2.1. Study Area. The field measurements were conducted in the city of Szeged (46.3°N, 20.1°E), the southeastern regional center of Hungary with an urbanized area of 40 km^2 [51]. Szeged offers an ideal study environment for urban climate and human-biometeorological investigations as it is built on a flat terrain with slight topographical differences (78–85 m above sea level), which enables the generalization of the obtained results, (see, e.g., [18, 52]). Urban land use patterns vary across the town, ranging from dense inner-city areas to sparse suburban landscapes, which allow for the development of several local climate zone types [53]. Szeged has a warm temperate climate with rather uniform annual distribution of precipitation. Based on the 1971–2000 climate normal data of Szeged, the yearly amount of precipitation is low (489 mm), while the number of sunshine hours is high (1978 h). The annual mean air temperature is 10.6°C, and July and August are the hottest months, while January is the coldest [54]. Being one of the warmest cities in Hungary, the urban climate of Szeged is expected to be affected intensively by the warming projected for the Carpathian Basin [55]. Moreover, Szeged is the third most populated city in the country with more than 162,000 permanent residents. These attributes make the city an appropriate place for urban climate and human-biometeorological investigations.

The medium-sized rectangular Bartók Square (Figure 1; core area: 110 m × 55 m, plus the surrounding streets) was selected as the study area for the field measurements and for the assessment of small-scale radiation models. The square is located within a "compact midrise" local climate zone (LCZ 2) in the inner-city [51]. It is an important hub of public transit and pedestrians traffic with two bus stops at its opposite sides. The square offers opportunities for recreation and socialization: there is an asphalt-covered basketball–football court on the WNW part, several small kiosks on the NNE side, and benches located across the place. Thus, the place serves the needs of people of all ages. The well-vegetated central and ESE parts of the square are characterized by 10–20 m tall deciduous trees (e.g., *Platanus* × *acerifolia, Tilia cordata, Ulmus procera, Sophora japonica, Fraxinus excelsior,* and *Celtis occidentalis*). Beside the shade from trees, parts of the square also benefit from the shading of the adjacent 3-4-story buildings.

Five measurement sites were selected to investigate the radiation load on pedestrians that either walk on the sidewalks surrounding the square or linger under the mature shade trees in the central area (Figure 2):

(i) P1, P2, P3, and P4 are located near to buildings encircling the square. The nearest façades to these points are located at SSW, WNW, NNE, and ESE sides, respectively, at ca. 1.3 m distance.

(ii) P5 is in the middle of the square, under a 10-meter tall *Sophora japonica* tree with an app. 13-meter wide crown; the station was placed 2 m north from the trunk of the tree.

2.2. Field Measurements. Two human-biometeorological stations were used to record one-minute averages of all atmospheric parameters influencing human thermal comfort (Figure 3). One of the stations was continuously moved around the four lateral measurement points (P1–P4) at 15-minute intervals, while the other remained under the large tree at point P5 during the entire measurement period. Both stations were equipped with a Vaisala WXT 520 weather transmitter to record air temperature (T_a), relative humidity,

FIGURE 1: Bartók Square of Szeged, illustrated by an aerial image, site photos, and an object elevation map.

and wind speed. They were also equipped with a rotatable Kipp & Zonen net radiometer to monitor the 3D radiant environment—that is, to record shortwave and longwave radiation flux densities from six perpendicular directions (K_i and L_i [Wm^{-2}], i: up, down, east, west, south, and north). By means of telescopic tripods, the sensors were set at 1.1–1.2 m above ground level—at an elevation recommended for human-biometeorological investigations [10].

Typically, in the first position, the arm of the net radiometers pointed to the south, while the sensors were faced upwards and downwards. This means that in this position, the two pyranometers and two pyrgeometers measured K_i and L_i separately from the upper and lower hemisphere (K_u, K_d, L_u, L_d). After three minutes, the net radiometers were rotated manually to the second position where the sensors faced east and west (K_e, K_w, L_e, L_w). After another 3-minute measurement, the arms were turned 90° to measure the radiation flux densities coming from the south and north (K_s, K_n, L_s, L_n). Considering our 26-hour measurement period, this procedure required hundreds of rotations. Taking into account the response time of the sensors, as well as the time delays due to rotation, the first K_i and L_i records following a rotation were removed. Additionally, to record conditions representative of a new thermal environment, the first three-minute data following relocations were also omitted.

Mean radiant temperature (T_{mrt} [°C]), a parameter with primary importance in the field of human-biometeorology, combines all longwave and shortwave radiant flux densities into a single value in °C. T_{mrt} is defined as the uniform temperature of an imaginary black body-radiating surrounding, which causes the same radiant heat exchange for the human body inside this hypothetical environment as the real, complex 3D radiant environment [11, 13]. In the case of this study, T_{mrt} was determined based on six K_i and six L_i flux densities obtained from three consecutive positions of the net radiometer.

$$T_{\mathrm{mrt}} = \sqrt[4]{\frac{K^* + L^*}{a_l \times \sigma}} - 273.15 \quad (1)$$

$$K^* = \sum K_i^* = \sum W_i \times a_k \times K_i \quad (2)$$

$$L^* = \sum L_i^* = \sum W_i \times a_l \times L_i \quad (3)$$

In (1), (2), and (3) K^* and L^* are the short- and longwave radiation load, that is, the sum of the absorbed short- and longwave radiation flux densities (K_i^*, L_i^*) of a clothed human-biometeorological reference person in standing position. a_k and a_l are the absorption coefficients of the clothed human body in the short- and longwave radiation domain (assumed to be 0.7 and 0.97, respectively), σ is the Stefan–Boltzmann constant ($5.67 \times 10^{-8}\,\mathrm{Wm}^{-2}\mathrm{K}^{-4}$), and W_i is a direction-dependent weighting factor. Assuming standing (or walking)

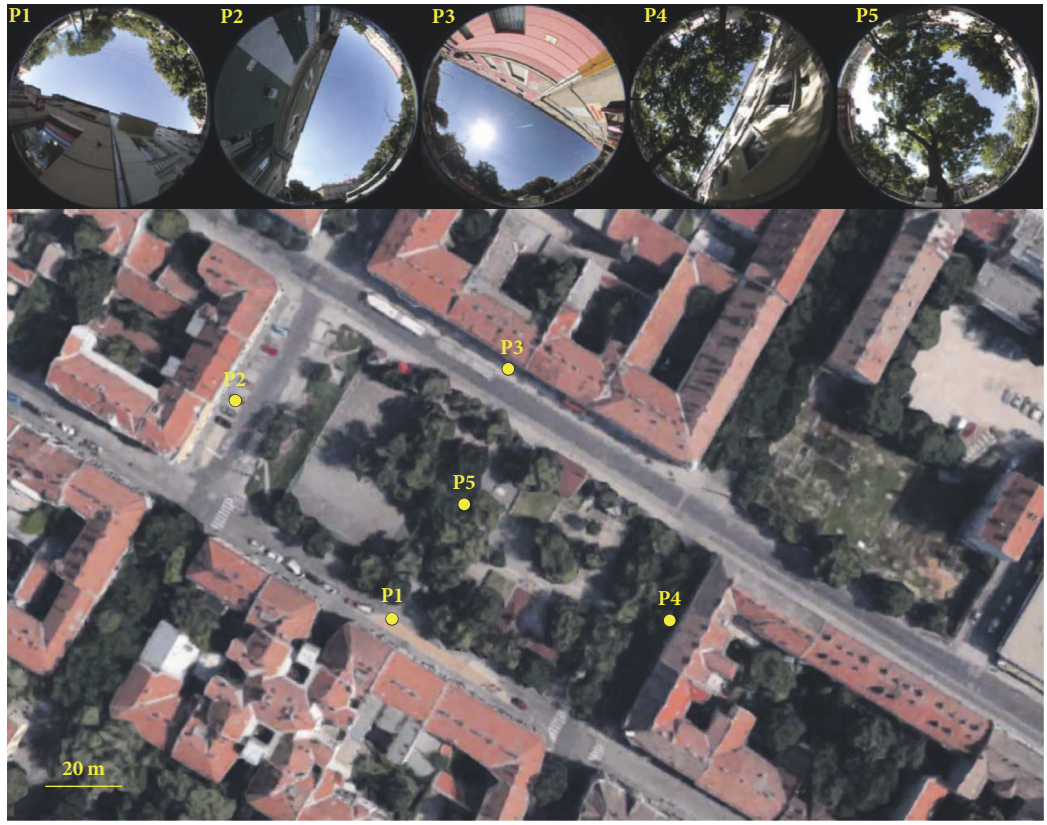

Figure 2: Survey points in the Bartók Square with their fish-eye photographs.

Figure 3: One of the human-biometeorological stations used in this study (photo taken at P3 site).

reference subject in this study, W_i is set as 0.06 for vertical and 0.22 for horizontal directions [11].

The 26-hour field campaign was conducted on two consecutive late-summer days with clear sky conditions (Figure 4). The measurement period started before sunset on August 7 and ended after sunset on August 8, 2016. According to the data obtained from the nearest urban weather station operated by the Hungarian Meteorological Service (HMS), the air temperature ranged from 17.1°C to 26.9°C during the measurement period, and the bell-shaped global radiation curve peaked at 848 Wm^{-2}. The clear and calm weather characterizing the measurement period supported the development of microclimate differences between the monitored sites to their fullest.

2.3. Numerical Models. Three numerical simulation models were assessed in their ability to reproduce radiation conditions in complex urban environments: ENVI-met (Version 4.0 Preview III), SOLWEIG (Version 2015a Beta), and RayMan Pro (Version 3.1 Beta). The study also utilized MATLAB and MS Excel for the analysis of the results.

The digital models of the square were developed utilizing (i) the GIS map of the city, (ii) the recent urban tree inventory of Szeged, based on a comprehensive field survey conducted

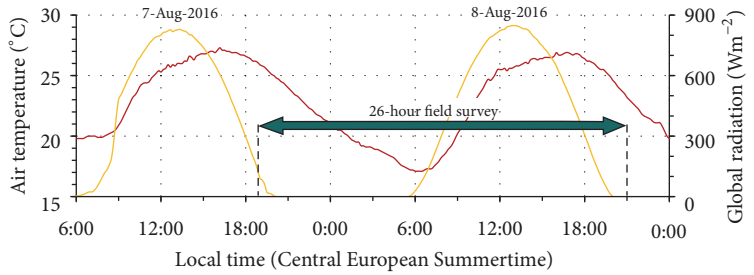

Figure 4: Background weather parameters (yellow: global radiation, red: air temperature) during the field measurements (10-min average data were obtained from the inner-city weather station of Szeged, 0.9 km away from the survey site).

by the Department of Climatology and Landscape Ecology, the University of Szeged [56, 57], and (iii) additional aerial analyses using Google Earth images and onsite surveys. As input weather data, each model utilized the 48-hour long (from August 7, 2016 to August 9, 2016) records from the nearest official weather station operated by the HMS. Each model ran for the same 48-hour period (starting from August 7, 2016) with model outputs saved at 15-minute intervals. The key numerical model specific settings are as follows.

In the case of ENVI-met, the 116 × 151 model area had a 3-meter horizontal resolution. Besides Bartók Square, the model domain encompassed the eight adjacent urban blocks as well. The vertical resolution utilized the telescopic setup. Here, the lowest four grids were set to 0.5 meter, while from 2 meter the height of each consequent grid increased by 20%. The top of the 3D model was at 105 m with the tallest building being 38 m. The model trees were selected from the software's predefined, species-specific, and three-dimensional tree catalogue by adjusting their physical shape and size only to match the surveyed values. The materials assigned to the ground surfaces were as follows: gravel asphalt to roads, sandy loam soil to urban blocks, and concrete pavement to paved surfaces within the square. The albedo of the gravel asphalt and the concrete surfaces was set to 0.25 and 0.35, respectively. The albedo of roofs and walls was set to 0.35, uniformly. In terms of atmospheric conditions, a simple model forcing was applied with air temperature and relative humidity values taken from the nearby urban weather station. In order to match the measured maximum global radiation values a solar adjustment factor of 0.98 was applied.

In the case of SOLWEIG, the digital surface models (DSMs) of buildings and tree canopies were derived from the city's GIS map using 1 meter resolution. The 477 × 424 digital model encompassed several streets and urban blocks around the square. Based on a long-term tree shade survey in Szeged [58, 59], the mean summer transmissivity value of 0.0678—calculated for the most common specie in Szeged, the *Celtis occidentalis*—was used in this study. The albedo of walls and ground was set to 0.35 and 0.25, respectively. The input meteorological data was compiled from the abovementioned urban weather station records.

Similarly to SOLWEIG, the files describing the three-dimensional physical environment in RayMan Pro were obtained from the city's GIS map. The process of generating digital models for RayMan requires the "Shp to Obs" plugin, which converts the coordinates of the observation points and that of the adjacent buildings and trees to the required format. The derived five digital models encompass 200 m × 200 m areas describing the surroundings of the observation points. In the same way as the other two models, the input weather data were obtained from the nearby urban weather station. In the simulations, the "reduction of global radiation (G [Wm^{-2}]) presetting by obstacles" function of the software was activated.

2.4. Numerical Model Assessment. The model evaluations were based on the 15-minute T_{mrt} data calculated from the field measurements and extracted from the numerical simulations. First, the model errors, that is, the differences between the model- and the measurement-based T_{mrt} values were calculated and illustrated.

$$\Delta T_{mrt} = T_{mrt(modeled)} - T_{mrt(measured)} \tag{4}$$

Then statistical evaluation of the utilized models was also implemented by calculating three parameters recommended by [60, 61]: the mean absolute error (MEA), the root mean square error (RMSE), and the index of agreement (IA).

$$\mathrm{MAE} = \frac{\sum \left| T_{mrt(modeled)} - T_{mrt(measured)} \right|}{n} \tag{5}$$

$$\mathrm{RMSE} = \sqrt{\frac{\sum \left(T_{mrt(modeled)} - T_{mrt(measured)} \right)^2}{n}} \tag{6}$$

$$\mathrm{IA} = 1 - \frac{\sum \left(T_{mrt(modeled)} - T_{mrt(measured)} \right)^2 / n}{\sum \left(\left| T_{mrt(modeled)} - \sum T_{mrt(modeled)} / n \right| + \left| T_{mrt(measured)} - \sum T_{mrt(measured)} / n \right| \right)^2 / n} \tag{7}$$

In (5), (6), and (7) n is the total number of the model-measurement data pairs, being 26 in the cases of P1, P2, P3, and P4, and 104 in the case of P5. The analyses were completed in Microsoft Excel. Simulation results can be regarded as reliable if the ΔT_{mrt}, MAE, and RMSE values are close to zero and if the IA value is close to 1.0.

3. Results and Discussion

3.1. Differences in Radiation Conditions within the Bartók Square. As illustrated by Figure 5, the temporal and spatial variation of shortwave radiation flux densities (K_i) were much greater than that of longwave flux densities (L_i). Following sunrise, K_i rose steadily from 0 Wm^{-2} and had a maximal value around 900 Wm^{-2} (see e.g., K_u at survey points P2 and P3). In contrast, all L_i components remained within a rather narrow range (between 360 and 600 Wm^{-2}) throughout the day in all cases. The highest values of K_u were measured in those parts of the Bartók Square that were exposed to direct radiation in the midday hours (P2, P3). Here the peak values of K_u were even higher than the global radiation measured at the nearby meteorological station, which may be explained with the reflected radiation components from the nearby façades. The relapses of K_i during their diurnal course clearly indicate the shading effect of buildings and trees at each measurement point, which, by affecting the energy budget of adjacent façades and pavement, indirectly also influences the heating up of surfaces and hence their emitted longwave radiation.

Due to its NNE exposure, P1 received direct solar radiation only for a brief period (see K_u and K_e curves at P1, Figure 5). Nevertheless, this short income was enough to warm up the adjacent surfaces so much that after a little delay the effect of irradiation became evident in the slightly elevated L_d values. Since P1 site and hence the adjacent façades were exposed to direct solar radiation only briefly, the surfaces did not become really significant sources of longwave radiation (in contrast to P2 and P3 points, discussed below). Consequently, there are only little differences between L_i components and the maximum of L_d still did not reach 500 Wm^{-2} at this survey point.

Due to its ESE exposure and lack of shading from trees, P2 received direct solar radiation for a long period (Figure 5). In the early morning the location received direct solar radiation from the north as well (see K_n values at P2). The fact that this point is well-exposed to solar radiation is indicated by its high K_u, K_e, and K_s values. However, by the time K_w component would have become significant, the site became shadowed by the adjacent building. In comparison to P1, P2 got a considerable amount of reflected radiation resulting in 100–200 Wm^{-2} high K_n, and K_w values during the day. In consequence of the ample solar radiation in the forenoon, the pavement and the ESE facing façade absorbed considerable energy and, by warming up, became effective sources of longwave radiation during the late forenoon and early afternoon hours. This is evident from the rather high (over 530 Wm^{-2}) L_d, L_w, and L_n values of P2. Due to the lack of shade, even L_s and L_e values are higher than in the case of P1, which remained shaded for most of the day; L_s peaked over 500 Wm^{-2} and the maximum L_e was around 485 Wm^{-2} at P2, whereas in the case of P1, these components remained below 470 Wm^{-2} during the entire measurement period.

P3, with its SSW exposure and without any trees to provide shade, received the greatest amount of solar radiation for the longest period (Figure 5). The undisturbed irradiation from ca. 10:00 until sunset is reflected in the consistently high K_u, K_e, K_s, and K_w values. Besides the direct solar radiation load, shortwave radiation reflected from the SSW-facing façade resulted in ca. 200 Wm^{-2} high K_n and K_e values in the afternoon. In the ESE-exposed P2 first K_e and then K_s became the dominant horizontal K_i component. In the case of the SSW-exposed P3 K_e was the leading horizontal shortwave component in the late forenoon, then K_s and finally K_w dominated over the entire afternoon. Due to the undisturbed and intensive irradiation, similarly to P2, longwave components at P3 have distinct runs. Rather high values can be observed in the case of L_d, L_n, and L_e (about 600, 565, and 560 Wm^{-2}, respectively). Even L_w and L_s can be regarded high (as a result of K_e irradiation in the forenoon L_w peaked above 500 Wm^{-2}).

Likewise, in the case of P4, we would expect a high irradiation load due to its WNW exposure (mainly because the adjacent building provided shade only until 13:00). However, due to the presence of a row of mature trees along the street shading the sidewalk during most of the afternoon, this location is characterized not only by the most obstructed sky view but also by the least amount of direct solar income (Figure 5). Direct irradiation occurred only around 14:00, which raised K_u, K_s, and K_w values at this site. Because of its WNW exposure, K_w component dominated among the shortwave flux densities during the late afternoon. However, while direct radiation resulted in 800 Wm^{-2} high K_w values at P3, in the absence of prolonged direct irradiation K_w component at P4 was constituted mainly by diffuse and reflected radiation that resulted in less than 200 Wm^{-2}. Unlike other observation points where L_u and L_d values had a distinct course (with typically lower L_u and generally higher L_d compared to the lateral flux densities), since P4 received a very low amount of direct solar radiation, its L_i components ran closely together during the day.

In the case of P5, located in the middle of the square and shaded by mature park trees, K_i and L_i components varied more than those at P4—the other survey point being shaded by trees (Figure 5). In the absence of nearby buildings, shade at P5 is only provided by trees, especially by a large *Sophora japonica* tree, under which the instrument was installed. However, this tree has a relatively high trunk height and provides effective shade only at high sun angles, therefore, direct solar radiation could reach the instrument periodically during the forenoon (K_e, K_u) and the afternoon (K_w, K_u). Due to these irradiations, the area below the tree warmed up more than that in the case of the more effectively sheltered P4. This explains the smaller peaks in the course of L_d at P5, which exceeded 500 Wm^{-2} for a short period.

At each site, exposure to direct solar radiation, meaning high K_u, K_e, K_s, and K_w values, increased the longwave radiation flux densities (L_d, L_w, L_n, and L_e) (Figure 5). The lowest L_i component was always observed from the partially

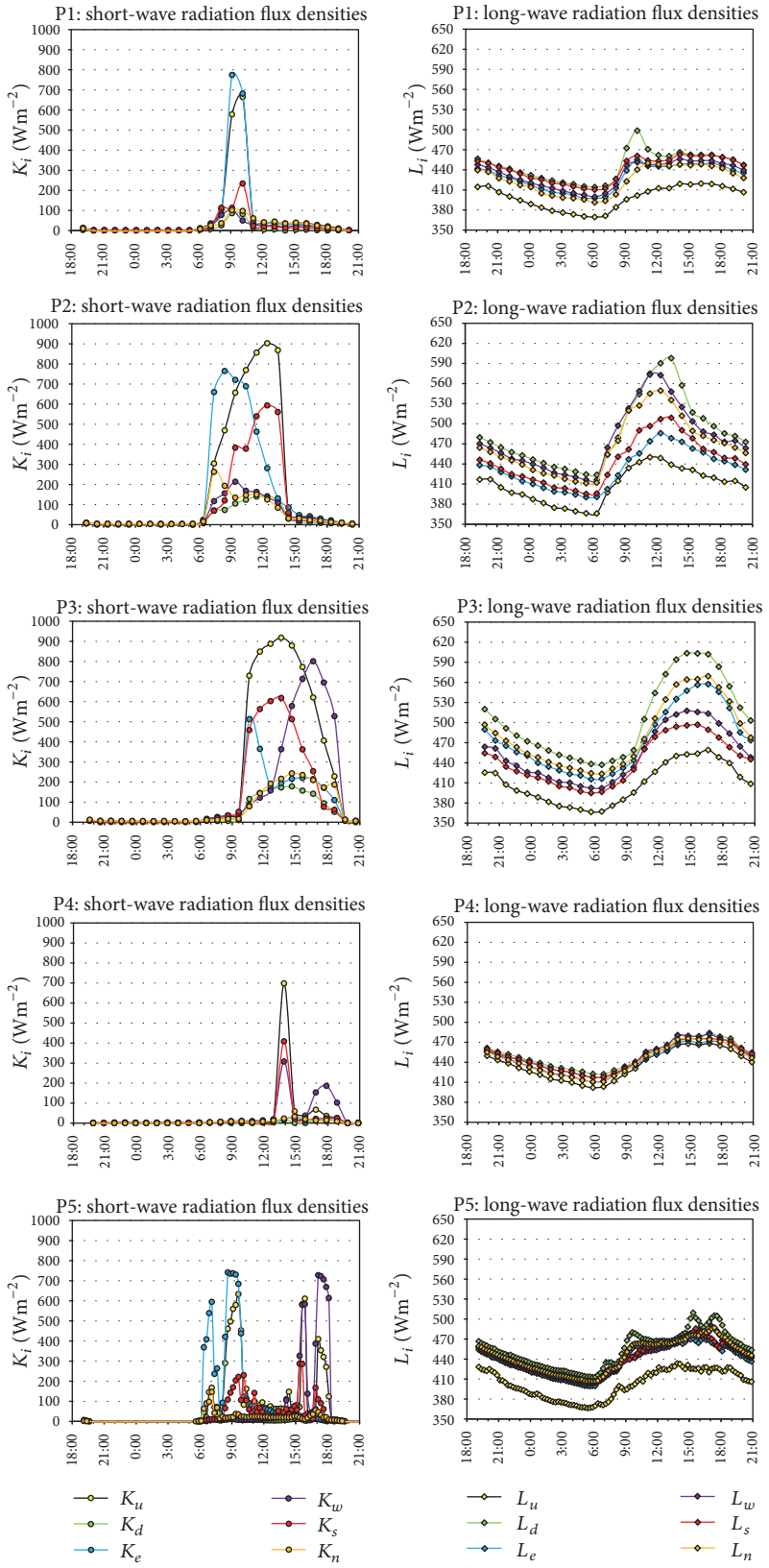

FIGURE 5: Short- (K_i) and longwave (L_i) radiation flux densities measured at the five survey points (note: to better illustrate the site-related differences different scales were applied for the short- and longwave domain).

obstructed "cold" sky (L_u). Longwave radiation components diverge in the case of P2 and P3, which received direct solar radiation for the longest period. In the case of P1 and P5, L_i curves (except for L_u) run together, while in the case of the sheltered P4, L_i components can hardly be distinguished.

Figure 6 illustrates the short- and longwave radiation flux densities absorbed by a standing or walking "reference person" (K_i^*, L_i^*), a typical subject usually assumed in human-biometeorological studies in the case of T_{mrt} calculations ($K_i^* = a_k \times W_i \times K_i$; $L_i^* = a_l \times W_i \times L_i$). The absorbed radiation components from the different directions are illustrated in a cumulative way to indicate the sum of absorbed short- and longwave radiation energy, that is, the short- and longwave radiation loads as well (K^*, L^*). Moreover, the same ordinate was adopted in the case of each short- and longwave graphical chart-pair to allow easy and accurate comparison of their contributions to the resulting whole radiation income of the human body (and therefore their role in the resulted T_{mrt}).

At night, in the absence of solar radiation, the radiation budget consists of longwave components only. Although L_i^* dominates daytime as well, the spatial and temporal differences in the whole radiation budget (and thus, in T_{mrt}) are primarily the result of the shortwave components (K_i^*). Due to the adopted directional-dependent weighting for a standing person, the influence of the vertical components (K_u, K_d, L_u, and L_d) decreases greatly. That is, if a person crosses the area or walks on the sidewalks by the buildings, then his/her radiation load originates primarily from lateral directions: mostly from direct solar radiation (K_e and/or K_s and/or K_w) and from the emitted longwave radiation of the irradiated façades (L_e, L_s, L_w, and L_n).

Figure 6 indicates the observed differences in radiation loads between the five measurement locations. People have to face the greatest radiation load at P3 and P2 points owing to both the orientation of adjacent façades (ESE and SSW) and the lack of shade trees or any artificial devices. During the day, the summed K^* is considerably high for a rather long time at these points: at P2 the maximum of K^* is around 250 Wm^{-2} (between 9:00 and 10:00), and at P3 the maximum K^* is around 280 Wm^{-2} (between 14:00 and 15:00) with four hours over 250 Wm^{-2}. Compared to K^*, L^* changes gradually with delayed peak values. L^* calculated for P2 reached its maximum around noon and exceeded 500 Wm^{-2} for two hours. In the case of P3, L^* exceeded 500 Wm^{-2} for over five hours, resulting in a maximum that extended over most of the afternoon. While L^* values exceeding 450 Wm^{-2} existed for about 8-9 hours at P2 and for 10 hours at P3, at other measurement locations L^* only briefly reached this value in the afternoon. In the case of P1, L^* remained considerably lower throughout the day. While low K^* and L^* values are primarily the result of the favorable NNE exposure of the P1 point, in the case of P4 and P5 the lower radiation income is the result of tree shading. It is worth emphasizing that with its WNW exposure, P4 would be subject to considerable radiation load over the afternoon if it would not be shaded by trees.

Figure 7 illustrates the obtained T_{mrt} values (as a result of the above discussed conditions), the air temperature (T_a) values and their differences ($T_{\mathrm{mrt}} - T_a$) for each site. In terms of T_a, there is little difference between the sites; during the night, the values remain within a 0.5°C range, whereas during the day, the greatest difference of 3°C is observed between the warmest P3 and the coldest P1 point. In contrast, T_{mrt} differences between the five sites are much greater. In terms of T_{mrt}, P3 is the warmest with a maximum of 74°C and with values over 70°C for four hours in the afternoon. The daily maximum remained somewhat lower (68°C) and occurred somewhat sooner in the case of P2. However, at P2 too, a prolonged, four-hour period with rather stressful conditions (values over 65°C) can be observed in the afternoon. In contrast, T_{mrt} at P1 remained below 30°C for the whole afternoon. In the case of the three mostly shaded points (P1, P4, and P5) the T_{mrt} values were closer to T_a and remained below 55°C even during the short irradiated periods.

For most of the day, there is little difference between T_a and T_{mrt} at P1. In the case of P4, T_{mrt} exceeds T_a by only a few degrees during the afternoon. At these points, the $T_{\mathrm{mrt}} - T_a$ difference grew only to about 31°C (P1) and 23°C (P4) during the short periods of irradiation. As a result of direct solar radiation in the forenoon and the afternoon, the $T_{\mathrm{mrt}} - T_a$ difference at P5 rose to the 20–30°C interval. In contrast, during high solar angles when the crown provided sufficient protection, this difference remained around 5°C. In the case of the most stressful locations (P2, P3), T_{mrt} exceeded T_a by over 40°C, conditions that persisted for about four hours.

3.2. Model Validation. Figure 8 presents the T_{mrt} values obtained through the different models in comparison with the measurement-based ones and the course of T_{mrt} model errors (ΔT_{mrt}). ΔT_{mrt} values were calculated for each observations site (P1–P5) and for each numerical model. T_{mrt} model errors were greater during the daytime than at night. Greater deviations from measured values generally occurred around sunrise and sunset because of differences in model resolutions. A good example to this error is the period from around 6:00 to 7:00 at P1, P2, and P3 sites. Here, ENVI-met (the coarsest model with 3 m × 3 m × 0.5 m resolution) lags behind SOLWEIG and RayMan Pro. To facilitate the visual analysis, the time of sunrise (SR) and sunset (SS), as well as the periods of direct solar radiation, are indicated at the bottom of each graph (Figure 8).

In general, extreme deviations (i.e., peaks and valleys) are the outcome of the mismatch between observed and modeled times when a given observation point becomes irradiated or shaded. A good example for this kind of error is the graph of P2. Here, ENVI-met's error curve dips at 8:00 (indicating that the place is still shaded according to the model), but it rebounces by 9:00 in the morning. Similarly, when the observation point becomes shaded in the afternoon at around 14:00, each model still indicates the presence of direct radiation and hence significantly overestimates the actual T_{mrt} values. Nevertheless, this extreme error disappears from the next observation in the following hour. These errors may arise either from coarse model resolutions or from differences between actual and modeled obstructing bodies (i.e., trees, buildings, or shading devices).

Besides the model-based errors (due to model inaccuracies and coarse model resolutions) other modeling error trends can also be deduced from the results:

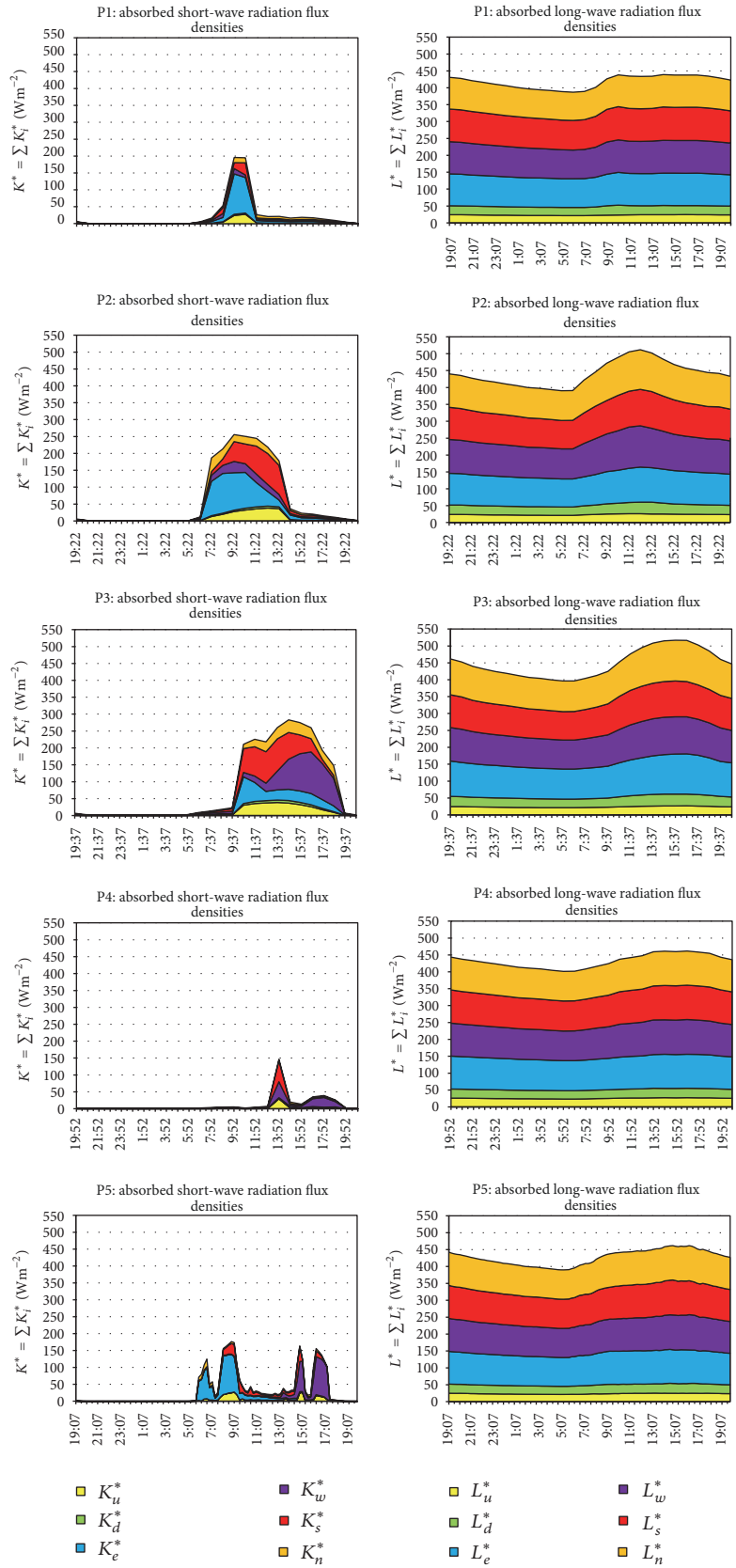

FIGURE 6: Sum of the short- (K_i^*) and longwave (L_i^*) radiation flux densities absorbed by the standing reference person at the five survey points (a_k: 0.7, a_l: 0.97, W_i: 0.06 for vertical directions and 0.22 for lateral directions).

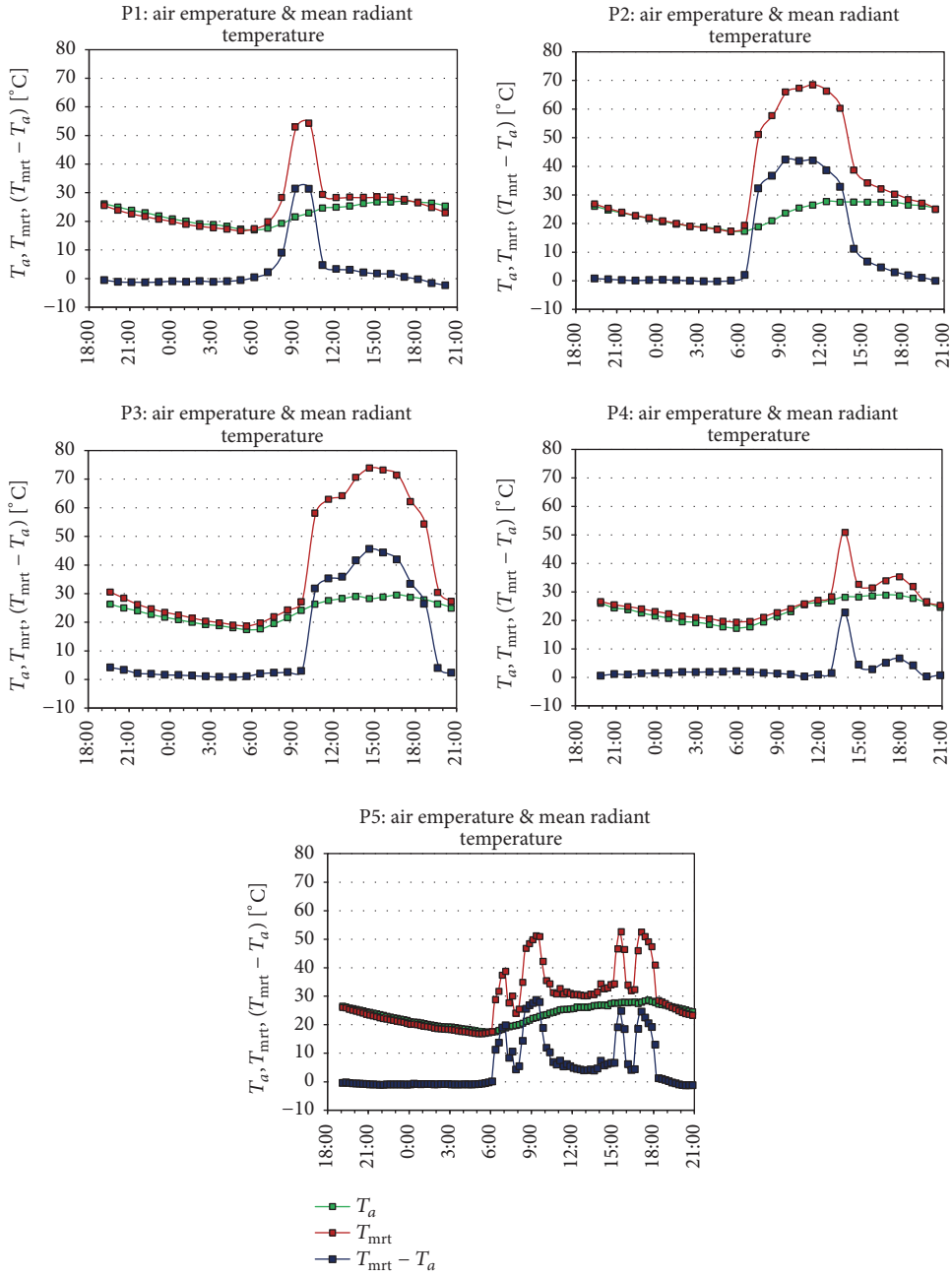

Figure 7: Air temperature (T_a), mean radiant temperature (T_{mrt}), and their differences at the five survey points.

(i) First, all models underestimate nighttime T_{mrt} by 5–10°C—except for SOLWEIG, in cases of sites that mostly remain shaded by trees (P4, P5).

(ii) Second, for those daylight hours when the survey points were shaded by buildings for a long time T_{mr} is generally overestimated by ENVI-met and SOLWEIG, whereas RayMan Pro hovers near or just below zero (P1, P4). For those daylight hours when the survey points were shaded by trees we can deduce similar trends, except for RayMan at P5. (At P5 T_{mr} is greatly overestimated by RayMan as a result of a subsequently discovered model glitch in which the modeled tree above the observation point lacks its crown. Although the imported obstacle file was correct, authors were not able to fix this unusual bug of RayMan in the case of this point).

(iii) Third, all models underestimate the daytime T_{mrt} when the observation points became irradiated by the sun and this is especially true for RayMan. In our validation, SOLWEIG and ENVI-met performed better in modeling the radiative conditions in these complex urban environments.

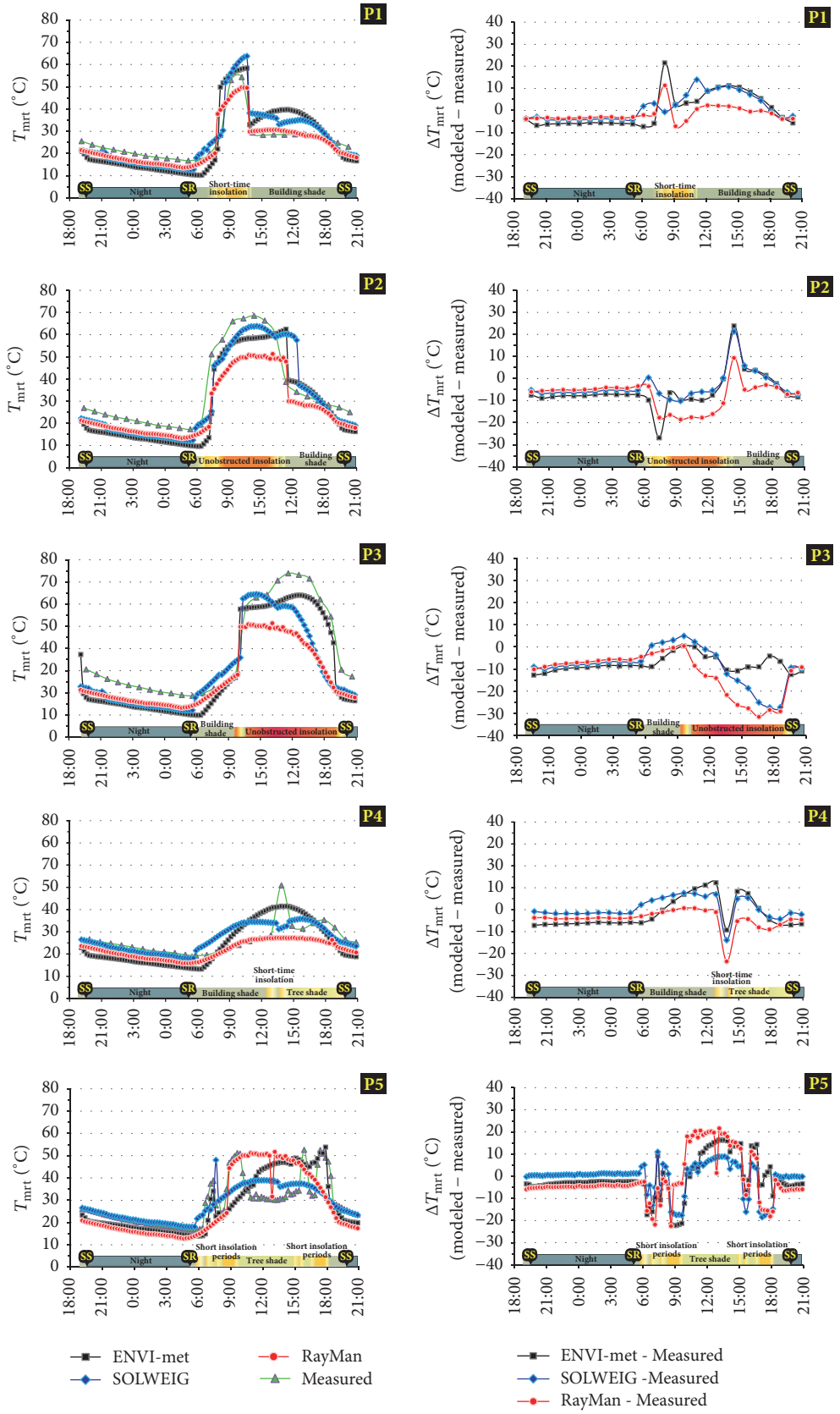

FIGURE 8: Deviation of the modeled T_{mrt} values from the measurement-based T_{mrt} at the five points during the survey period (SS: sunset, SR: sunrise; note: data are calculated from 15-minute averages). Horizontal bars at the bottom of each graph indicate when the measurement point became shaded or exposed to the sun as follows: (i) yellow and orange colors mark shorter and longer periods of solar exposure, respectively; (ii) light green indicates period of shade from trees; (iii) dark green suggests shade from buildings; (iv) dark gray signals nighttime with no short-wave radiation. SS and SR marks indicate times of sunset and sunrise, respectively.

Table 1: Summary of the statistical analysis.

		Six-directional measurements		
		ENVI-met	SOLWEIG	RayMan
MAE	P1	6.68	5.00	3.13
	P2	8.27	6.03	8.09
	P3	7.85	9.58	11.61
	P4	6.45	3.74	4.40
	P5	6.67	4.58	8.58
RMSE	P1	7.67	5.92	3.82
	P2	9.94	7.15	9.71
	P3	8.56	12.06	14.91
	P4	6.94	4.80	6.23
	P5	8.90	7.09	10.58
IA	P1	0.89	0.92	0.96
	P2	0.93	0.96	0.91
	P3	0.96	0.90	0.83
	P4	0.80	0.84	0.67
	P5	0.82	0.81	0.78

Table 1 summarizes the calculated statistic of the models' performance separately for each survey point. Taking into account the MAE and RMSE values, the largest discrepancies can be observed at P3, the mostly irradiated survey point. The best model performance (i.e., the smallest MAE and RMSE values) was achieved by SOLWEIG in the case of P4, P2, and P5, while at P1 RayMan and at P3 ENVI-met performed the best. For ENVI-met, we cannot observe large variations among the survey points; MAE values are between 6.45 (P4) and 8.27 (P2), while the corresponding RMSE values are 6.94 and 9.94. In the cases of SOLWEIG and RayMan much greater variations can be detected among the survey points. The lowest MAE and RMSE values were achieved in the case of the mostly shaded survey point of P4 (best model performance) and the greatest MAE and RMSE values were calculated for the most irradiated survey point P3 (worst model performance), probably because the utilized models are unable to handle the irradiated and thus warmed surfaces' prolonged heat emitting effect.

For IA, values close to 1.0 indicate better model performance. The highest index of agreements was achieved by SOLWEIG in P2 and P4 locations, whereas ENVI-met excelled at P3 and P5 points. In the case of P1, RayMan's results were closest to the measured values. In terms of IA, models performed better in the case of the survey points without tree shade. At P1, P2, and P3 the IA values were generally close to or above 0.9, while in the presence of tree shade (P4, P5) IA values were always below 0.85. The lowest IA (0.67) was obtained in the case of P4 by simulations with the RayMan. A comparatively good IA of 0.96 was achieved by RayMan at P1, by SOLWEIG at P2, and by ENVI-met at P3.

Taking into account all of the abovementioned analyses (graphical analyses of Figure 8 and computed statistics in Table 1), SOLWEIG showed the best performance among the evaluated models. ENVI-met delivered a comparable performance to SOLWEIG. However, due to the applied coarse digital model resolution, ENVI-met slightly underperformed compared to the former.

Figure 9 indicates the achievements of this model validation study in the light of the earlier researches. Direct comparison of the study outcomes is extremely difficult due to the differences in the adopted simulation models, model versions, modeling options, validation techniques, survey periods, and adopted methods and measures to indicate the performance of the models. For example, although there are a couple of validation studies in the case of the RayMan model, some of them adopted the radically different globe thermometer-based "Tg-technique" to obtain experimental T_{mrt} data. Moreover, in the case of the same validation technique of six-directional measurements, neither of the listed validation studies utilized the obstacle file modeling option of RayMan. Instead, they relied on the more easily achievable option of importing the fish-eye photos of the survey points. In this study we opted for the usage of the obstacle file to make the outcomes of RayMan validation comparable with the other simulation software. As emphasized by [42], the results of the existing T_{mrt} validations available are inconsistent, and thus, there is a need for the standardization of model-validation processes.

4. Conclusions

With an urban population of around 75%, and especially in the light of the aging population in European countries, reduction of the adverse effects of heat waves and maintenance of comfortable conditions within cities are extremely important issues for urban planning and landscape design. Human-biometeorological studies, conducted in Central European cities, shed light on the leading role of radiation conditions in the development of summertime heat stress. Up till now, however, only a limited number of field investigations aiming to map at fine spatial and temporal resolution the variations of heat stress owing to the landscape design have been conducted. Nonetheless, their results demonstrate the potential of climate-conscious and climate-adaptive urban planning and can be used to validate the results of numerical simulations.

Our complex study comprising field measurements and numerical simulations was undertaken to investigate radiative conditions and their modeled reproduction at a complex urban environment over a 26-hour period in Szeged, Hungary. The field measurement data obtained from five measurement points were compared and the performance of three commonly available microclimate models in reproducing T_{mrt} values was assessed.

The measurements confirmed that on clear summer days T_{mrt} can reach an extreme level at exposed locations (65–75°C). Nevertheless, shade by mature trees is able to reduce the daytime T_{mrt} to 30–35°C. Shading from buildings adjacent to sidewalks plays an important role in reducing pedestrian heat stress, but this works only when façades are located SE, S, or SW to sidewalks, that is, when the sidewalk is open to NW, N, or NE. Therefore, it is extremely important

Reference	City	Sites	Site characteristics	Date/period	Time of the day	Sky cover	Model (and version)	Main option applied during the modeling	Validation technique	Visual comparison	Linear regression			Calculated statistics			
											a	*b*	R^2	*R*	RMSE	MAE	IA
Ali-Toudert 2005 [37]	Freiburg (Germany)	1	E-W street canyon N (S-exposed) sidewalk	July 14-15, 2003	10:00–12:00 LST (26 hours)	Clear sky	ENVI-met 3.0	Obstacle file + 0.84 adjusting factor for *G*	6-dir technique	Yes	*n.a.*	*n.a.*	*n.a.*	*n.a.*	*n.a.*	*n.a.*	*n.a.*
Huttner 2012 [38]	Freiburg (Germany)	1	E-W street canyon N (S-exposed) sidewalk	May 24, 2007	8:00-8:00 CET	Clear sky	ENVI-met 3.1	Obstacle file + forced meteorological input data	6-dir technique	Yes	*n.a.*	*n.a.*	*n.a.*	*n.a.*	4.00	*n.a.*	*n.a.*
		1	Vauban, N-oriented sidewalk	July 15, 2007	9:00–18 (CET)	Clear sky				*No*					5.00		
Thorsson et al. 2007 [12]	Göteborg (Sweden)	1	A large open square	July 26, 2006	4:00–20:30 LST	Clear sky	RayMan 1.2	Without importing obstacles or fish-eye photo	6-dir technique	Yes	*n.a.*	*n.a.*	*n.a.*	*n.a.*	*n.a.*	*n.a.*	*n.a.*
				October 11, 2005	6:30–17:20 LST	Clear sky											
Matzarakis et al. 2007 [40]	Freiburg (Germany)	5	P1: E-W street canyon N sidewalk P2: E-W street canyon S sidewalk P3: N-S street canyon E sidewalk P4: N-S street canyonWsidewalk P5: under a mighty tree crown	August 2, 2001	5:00–22:00 CET	Clear sky	RayMan 1.2	Importing fish-eye photo	6-dir technique	*No*	0.95	1.61	0.77	*0.88*	*n.a.*	*n.a.*	*n.a.*
Matzarakis et al. 2010 [41]	Freiburg (Germany)	2	P1: under a group of trees	July 17, 18, 19, 2006	6:00–20:00 CET	Clear sky	RayMan 1.2	Importing fish-eye photo	6-dir technique	Yes	1.20	−7.70	*0.92*	0.96	0.70	*n.a.*	*n.a.*
			P2: a semiopen space			Clear sky					1.06	−6.20	*0.90*	0.95	3.70		
Lin et al. 2010 [22]	Huwei (Taiwan)	6	P1–P5: outdoor spaces with different shading levels P6: on the roof of a 4-storey building	May 16, 2007 August 15, 2006 November 20, 2007 January 8, 2008	8:00–18:00 LST	Variable	RayMan 1.2	Importing fish-eye photo	Tg-technique	Yes	0.92	2.18	0.85	*0.92*	*n.a.*	*n.a.*	*n.a.*
Hwang et al. 2011 [49]	Huwei (Taiwan)	7	P1–P6: outdoor spaces with different shading levels P7: on the roof of a 10 m high building	March 22, 2009 August 1, 2009 October 18, 2008 January 11, 2009	8:00–18:00 LST	Variable	RayMan 1.2	Importing fish-eye photo	Tg-technique	Yes *No*	0.96	1.98	0.88	*0.94*	*n.a.*	*n.a.*	*n.a.*
Krüger et al. 2014 [48]	Glasgow (Scotland)	6	Sites without tree shade: 3 sites in street canyons 3 sites at crossroads	19 days between March and July 2011	10–13 LST	Clear and intermediate sky	RayMan Pro	Urban: Ta, RH, v, *G*	Tg-technique	Yes	*n.a.*	*n.a.*	*0.45*	0.67	11.60	9.30	0.69
								Urban: Ta, RH, v + fish-eye photo + rural: *G*			*n.a.*	*n.a.*	*0.08*	0.28	11.90	9.90	0.54
								Urban: Ta, RH, v + fish-eye photo (without *G*)			*n.a.*	*n.a.*	*0.00*	0.03	20.20	18.00	0.37
								Urban: Ta, RH, v + rural: *G* (without fish-eye photo)			*n.a.*	*n.a.*	*0.24*	0.49	16.00	14.30	0.51
Lee & Mayer 2016 [42]	Freiburg (Germany)	5	ESE-WNW street canyon, SSW-facing sidewalk P1–P4: sites under tree crowns of different dimensions and densities P5: completely sunlit site	July 27, 2009	10–16 CET	Clear sky	RayMan Pro 2.0	Importing fish-eye photo	Tg-technique	*No*	0.29	37.50	0.40	*0.63*	12.63	*n.a.*	0.64
Lee et al. 2016 [30]	Freiburg (Germany)	5	ESE-WMW street canyon, SSW-facing sidewalk P1–P4: sites under tree crowns of different dimensions and densities	July 27, 2009	10–16 CET	Clear sky	RayMan Pro 2.0	Importing fish-eye photo	6-dir technique	*No*	0.29	37.50	0.40	*0.63*	12.63	*n.a.*	0.64
							ENVI-met 4.0 & BioMet 1.0	Obstacle file + forced meteorological input data			1.05	0.30	0.86	*0.93*	5.49	*n.a.*	0.95
Chen et al. 2014 [47]	Freiburg (Germany)	1	Grassland	August 10, 2010	8:00–16:00 CET	Clear morning, cloudy afternoon	RayMan Pro 2.0	*G* measured at 1.1 m agl	6-dir technique	Yes	1.89	−51.34	*0.81*	0.90	*n.a.*	*n.a.*	*n.a.*
								Importing fish-eye photo + *G* measured on the roof			1.28	−22.44	*0.77*	0.88			
							ENVI-met	Obstacle file + no imported global radiation			5.88	−263.59	*0.06*	0.25			
							SOLWEIG 2.1	Obstacle file + hourly *G* measured on the roof			1.54	−31.05	*0.32*	0.57			
This study	Szeged (Hungary)	5	Medium-sized rectangular square P1–P4: along the bordering façades P1: NNE-facing sidewalk, without tree shade P2: ESE-facing sidewalk, without tree shade P3: SSW-facing sidewalk, without tree shade P4: WNW-facing sidewalk, with tree shade P5: middle of the square, with tree shade	August 7-8, 2016	19:00–21:00 LST (26 hours)	Clear sky	RayMan Pro 3.1 Beta	Obstacle file + *G* measured on the roof	6-dir technique	Yes	*n.a.*	*n.a.*	*n.a.*	*n.a.*	9.05	7.16	0.83
							ENVI-met 4.0 Preview III	Obstacle file + *G* measured on the roof			*n.a.*	*n.a.*	*n.a.*	*n.a.*	8.40	7.18	0.88
							SOLWEIG 2015a Beta	Obstacle file + *G* measured on the roof			*n.a.*	*n.a.*	*n.a.*	*n.a.*	7.40	5.78	0.89

Figure 9: Data extracted from previous model validation studies (*6-dir* technique: filed measurements utilizing pyranometers and pyrgeometers (or net radiometers as an alternative) to obtain short-and long-wave radiation flux densities from six perpendicular directions; Tg-technique: field measurements utilizing globe-thermometers together with air temperature and wind velocity measurements; *a* and *b*: coefficients of linear regressions $T_{mrt(modeled)} = a \times T_{mrt(measured)} + b$; R^2: coefficient of determination; *R*: Pearson's correlation coefficient; RMSE: root mean square error; MAE: mean absolute error; IA: Willmott's index of agreement; note: n.a. as well as other cells written in italics font indicate data that were not available in the cited studies).

to shade by trees or artificial devices those sidewalks that face SE, S, and SW, because they do not benefit from the shading effect of buildings. When a measurement point adjacent to a façade becomes exposed to direct solar radiation, the radiation load increases significantly due to the additional lateral components, in some extent due to the reflected shortwave radiation (from the building wall), but in a great extent due to the emitted longwave radiation of the heated façade.

The numerical model assessment found that models generally underestimate the nighttime T_{mrt} by 5–10°C, except for SOLWEIG in locations where shade trees were present (P4, P5). Similarly, each model underestimates the daytime radiant conditions when the observation points became exposed to direct solar radiation. In contrast, ENVI-met and SOLWEIG generally overestimate, while RayMan Pro is most accurate in reproducing daytime T_{mrt} values in shade. (Except for P5 where an inexplicable model glitch has been identified which may be one of the shortcomings of the adopted RayMan model version.) Most of the extreme model errors (peaks and valleys) are the results of model inaccuracies and coarse model resolutions. Additionally, the measurement–model comparison revealed minor discrepancies that originated from the models' treatment of tree crowns: in the case of SOLWEIG and RayMan they were represented as perfectly shaped and having homogeneous bodies. Due to these simplifications, the occasional penetrations of direct sunbeams through the canopy observed at most locations were not reproduced.

Our study demonstrates that detailed field measurements can enhance our understanding of microclimatic conditions at a fine-scale, which, in turn, can be used by landscape designers and architects for climate-responsive urban design. Recent planning directives of the European Commission (EC) gave priority to nature-based solutions (NBS) and hence to renaturing cities [62]. NBS is a recently introduced concept in environmental research and management that promotes nature as a means to address the challenges brought about by climate change. Within the scope of the international Nature4Cities project (https://www.nature4cities.eu) fostering the use of NBS within urban areas, an inter- and cross-disciplinary research is conducted to assess the performance of archetypal nature-based solutions (different types of green walls, green roofs, urban trees, parks, etc.) for addressing various urban challenges such as mitigating heat in urban areas. In European cities, especially in those with dense historic urban cores, carefully planned and properly

maintained shade trees constitute the most effective NBS for mitigating extreme thermal conditions, while also offering several cobenefits.

Conflicts of Interest

There are no conflicts of interest related to this paper.

Acknowledgments

The presented analyses were conducted within the frame of the Nature4Cities project, which has received funding from the European Union's Horizon 2020 research and innovation programme under Grant agreement no. 730468. This research was supported by the EU-funded Hungarian Grant EFOP-3.6.1-16-2016-00008. The authors would like to express their gratitude for those who supported the field measurements, especially Gábor Horváth, Márton Kiss, Ágnes Takács, and Zsuzsa Győri.

References

[1] R. S. Kovats, R. Valentini, E. Bouwer et al., *Climate Change 2014: Impacts, Adaptation, And Vulnerability. Part B: Regional Aspects. Contribution of Working Group II to The Fifth Assessment Report of The Intergovernmental Panel on Climate Change*, V. R. Barros et al., Ed., Cambridge University Press, Cambridge, UK, 2014.

[2] J. Bartholy, R. Pongrácz, and I. Pieczka, "How the climate will change in this century?" *Hungarian Geographical Bulletin*, vol. 63, no. 1, pp. 55–67, 2014.

[3] I. D. Stewart and T. R. Oke, "Local climate zones for urban temperature studies," *Bulletin of the American Meteorological Society*, vol. 93, no. 12, pp. 1879–1900, 2012.

[4] S. N. Seo, "Urban adaptation to climate change in Europe," Transforming cities in a changing climate 12/2016, 2016.

[5] H. Mayer, "Urban bioclimatology," *Experientia*, vol. 49, no. 11, pp. 957–963, 1993.

[6] A. Ishigami, S. Hajat, R. S. Kovats et al., "An ecological time-series study of heat-related mortality in three European cities," *Environmental Health: A Global Access Science Source*, vol. 7, article no. 5, 2008.

[7] UN United Nations, *Department of Economic and Social Affairs, Population Division (2015)*, Department of Economic and Social Affairs, Population Division, Highlights, 2015.

[8] I. Eliasson, "The use of climate knowledge in urban planning," *Landscape and Urban Planning*, vol. 48, no. 1-2, pp. 31–44, 2000.

[9] G. Mills, "Progress toward sustainable settlements: a role for urban climatology," *Theoretical and Applied Climatology*, vol. 84, no. 1-3, pp. 69–76, 2006.

[10] H. Mayer, J. Holst, P. Dostal, F. Imbery, and D. Schindler, "Human thermal comfort in summer within an urban street canyon in Central Europe," *Meteorologische Zeitschrift*, vol. 17, no. 3, pp. 241–250, 2008.

[11] P. Höppe, *Ein Neues Verfahren Zur Bestimmung Der Mittleren Strahlungstemperatur in Freien*, vol. 44, Wetter und Leben, 1992.

[12] S. Thorsson, F. Lindberg, I. Eliasson, and B. Holmer, "Different methods for estimating the mean radiant temperature in an outdoor urban setting," *International Journal of Climatology*, vol. 27, no. 14, pp. 1983–1993, 2007.

[13] N. Kántor and J. Unger, "The most problematic variable in the course of human-biometeorological comfort assessment - The mean radiant temperature," *Central European Journal of Geosciences*, vol. 3, no. 1, pp. 90–100, 2011.

[14] F. Ali-Toudert, M. Djenane, R. Bensalem, and H. Mayer, "Outdoor thermal comfort in the old desert city of Beni-Isguen, Algeria," *Climate Research*, vol. 28, no. 3, pp. 243–256, 2005.

[15] F. Ali-Toudert and H. Mayer, "Numerical study on the effects of aspect ratio and orientation of an urban street canyon on outdoor thermal comfort in hot and dry climate," *Building and Environment*, vol. 41, no. 2, pp. 94–108, 2006.

[16] F. Ali-Toudert and H. Mayer, "Effects of asymmetry, galleries, overhanging façades and vegetation on thermal comfort in urban street canyons," *Solar Energy*, vol. 81, no. 6, pp. 742–754, 2007.

[17] F. Ali-Toudert and H. Mayer, "Thermal comfort in an east-west oriented street canyon in Freiburg (Germany) under hot summer conditions," *Theoretical and Applied Climatology*, vol. 87, no. 1–4, pp. 223–237, 2007.

[18] Á. Gulyás, J. Unger, and A. Matzarakis, "Assessment of the microclimatic and human comfort conditions in a complex urban environment: modelling and measurements," *Building and Environment*, vol. 41, no. 12, pp. 1713–1722, 2006.

[19] R. Emmanuel, H. Rosenlund, and E. Johansson, "Urban shading—a design option for the tropics? A study in Colombo, Sri Lanka," *International Journal of Climatology*, vol. 27, no. 14, pp. 1995–2004, 2007.

[20] J. Holst and H. Mayer, "Urban human-biometeorology: investigations in Freiburg (Germany) on human thermal comfort," *Urban Climate News*, vol. 38, pp. 5–10, 2010.

[21] J. Holst and H. Mayer, "Impacts of street design parameters on human-biometeorological variables," *Meteorologische Zeitschrift*, vol. 20, no. 5, pp. 541–552, 2011.

[22] T.-P. Lin, A. Matzarakis, and R.-L. Hwang, "Shading effect on long-term outdoor thermal comfort," *Building and Environment*, vol. 45, no. 1, pp. 213–221, 2010.

[23] V. M. Gómez-Muñoz, M. A. Porta-Gándara, and J. L. Fernández, "Effect of tree shades in urban planning in hot-arid climatic regions," *Landscape and Urban Planning*, vol. 94, no. 3-4, pp. 149–157, 2010.

[24] L. Shashua-Bar, D. Pearlmutter, and E. Erell, "The influence of trees and grass on outdoor thermal comfort in a hot-arid environment," *International Journal of Climatology*, vol. 31, no. 10, pp. 1498–1506, 2011.

[25] L. Shashua-Bar, I. X. Tsiros, and M. Hoffman, "Passive cooling design options to ameliorate thermal comfort in urban streets of a Mediterranean climate (Athens) under hot summer conditions," *Building and Environment*, vol. 57, pp. 110–119, 2012.

[26] N. Makaremi, E. Salleh, M. Z. Jaafar, and A. GhaffarianHoseini, "Thermal comfort conditions of shaded outdoor spaces in hot and humid climate of Malaysia," *Building and Environment*, vol. 48, no. 1, pp. 7–14, 2012.

[27] L. V. de Abreu-Harbich, L. C. Labaki, and A. Matzarakis, "Effect of tree planting design and tree species on human thermal comfort in the tropics," *Landscape and Urban Planning*, vol. 138, pp. 99–109, 2015.

[28] H. Lee, J. Holst, and H. Mayer, "Modification of human-biometeorologically significant radiant flux densities by shading as local method to mitigate heat stress in summer within urban street canyons," *Advances in Meteorology*, vol. 2013, Article ID 312572, 13 pages, 2013.

[29] H. Lee, H. Mayer, and D. Schindler, "Importance of 3-D radiant flux densities for outdoor human thermal comfort

on clear-sky summer days in Freiburg, Southwest Germany," *Meteorologische Zeitschrift*, vol. 23, no. 3, pp. 315–330, 2014.

[30] H. Lee, H. Mayer, and L. Chen, "Contribution of trees and grasslands to the mitigation of human heat stress in a residential district of Freiburg, Southwest Germany," *Landscape and Urban Planning*, vol. 148, pp. 37–50, 2016.

[31] S. Saneinejad, P. Moonen, and J. Carmeliet, "Comparative assessment of various heat island mitigation measures," *Building and Environment*, vol. 73, pp. 162–170, 2014.

[32] C. O'Malley, P. Piroozfar, E. R. P. Farr, and F. Pomponi, "Urban Heat Island (UHI) mitigating strategies: a case-based comparative analysis," *Sustainable Cities and Society*, vol. 19, article no. 284, pp. 222–235, 2015.

[33] C. V. Gál, "Urban greening and cool surfaces: the effectiveness of climate change adaptation strategies within the context of Budapest," in *Proceedings of ICUC9, 9th International Conference on Urban Climate jointly with the 12th Symposium on the Urban Environment*, Toulouse, France, July 2015.

[34] N. Kántor, A. Kovács, and Á. Takács, "Small-scale human-biometeorological impacts of shading by a large tree," *Open Geosciences*, vol. 8, no. 1, pp. 231–245, 2016.

[35] M. Bruse and H. Fleer, "Simulating surface-plant-air interactions inside urban environments with a three dimensional numerical model," *Environmental Modeling and Software*, vol. 13, no. 3-4, pp. 373–384, 1998.

[36] M. Bruse, "ENVI-met 3.0: updated model overview," http://envi-met.net/documents/papers/.

[37] F. Ali-Toudert, *Dependence of outdoor thermal comfort on street design in hot and dry climate [Ph.D. thesis]*, Universität Freiburg, Freiburg, Germany, 2005.

[38] S. Huttner, *Further development and application of the 3D micro-climate simulation ENVI-met [Ph.D. thesis]*, Johannes Gutenberg-Universitat Mainz, Mainz, Germany, 2012.

[39] H. Simon, *Modeling urban microclimate: development, implementation and evaluation of new and improved calculation methods for the urban microclimate model envi-met [Ph.D. thesis]*, Johannes Gutenberg-Universitat Mainz, Mainz, Germany, 2016.

[40] A. Matzarakis, F. Rutz, and H. Mayer, "Modelling radiation fluxes in simple and complex environments—application of the RayMan model," *International Journal of Biometerology*, vol. 51, no. 4, pp. 323–334, 2007.

[41] A. Matzarakis, F. Rutz, and H. Mayer, "Modelling radiation fluxes in simple and complex environments: basics of the RayMan model," *International Journal of Biometerology*, vol. 54, no. 2, pp. 131–139, 2010.

[42] H. Lee and H. Mayer, "Validation of the mean radiant temperature simulated by the RayMan software in urban environments," *International Journal of Biometerology*, vol. 60, no. 11, pp. 1775–1785, 2016.

[43] F. Lindberg, B. Holmer, and S. Thorsson, "SOLWEIG 1.0—modelling spatial variations of 3D radiant fluxes and mean radiant temperature in complex urban settings," *International Journal of Biometerology*, vol. 52, no. 7, pp. 697–713, 2008.

[44] F. Lindberg and C. S. B. Grimmond, "The influence of vegetation and building morphology on shadow patterns and mean radiant temperatures in urban areas: model development and evaluation," *Theoretical and Applied Climatology*, vol. 105, no. 3-4, pp. 311–323, 2011.

[45] F. Lindberg, S. Onomura, and C. S. B. Grimmond, "Influence of ground surface characteristics on the mean radiant temperature in urban areas," *International Journal of Biometerology*, vol. 60, no. 9, pp. 1439–1452, 2016.

[46] J. Konarska, F. Lindberg, A. Larsson, S. Thorsson, and B. Holmer, "Transmissivity of solar radiation through crowns of single urban trees-application for outdoor thermal comfort modelling," *Theoretical and Applied Climatology*, vol. 117, no. 3-4, pp. 363–376, 2014.

[47] Y.-C. Chen, T.-P. Lin, and A. Matzarakis, "Comparison of mean radiant temperature from field experiment and modelling: a case study in Freiburg, Germany," *Theoretical and Applied Climatology*, vol. 118, no. 3, pp. 535–551, 2014.

[48] E. L. Krüger, F. O. Minella, and A. Matzarakis, "Comparison of different methods of estimating the mean radiant temperature in outdoor thermal comfort studies," *International Journal of Biometerology*, vol. 58, no. 8, pp. 1727–1737, 2014.

[49] R.-L. Hwang, T.-P. Lin, and A. Matzarakis, "Seasonal effects of urban street shading on long-term outdoor thermal comfort," *Building and Environment*, vol. 46, no. 4, pp. 863–870, 2011.

[50] S. Wang and Y. Li, "Suitability of acrylic and copper globe thermometers for diurnal outdoor settings," *Building and Environment*, vol. 89, pp. 279–294, 2015.

[51] E. Lelovics, J. Unger, T. Gál, and C. V. Gál, "Design of an urban monitoring network based on Local Climate Zone mapping and temperature pattern modelling," *Climate Research*, vol. 60, no. 1, pp. 51–62, 2014.

[52] J. Unger, "Heat island intensity with different meteorological conditions in a medium-sized town: Szeged, Hungary," *Theoretical and Applied Climatology*, vol. 54, no. 3-4, pp. 147–151, 1996.

[53] J. Unger, E. Lelovics, and T. Gál, "Local climate zone mapping using GIS methods in Szeged," *Hungarian Geographical Bulletin*, vol. 63, no. 1, pp. 29–41, 2014.

[54] HMS Hungarian Meteorological Service, "Climate characteristics of Szeged," 2015, http://www.met.hu/eghajlat/magyarorszag_eghajlata/varosok_jellemzoi/Szeged/.

[55] R. Pongrácz, J. Bartholy, and E. B. Bartha, "Analysis of projected changes in the occurrence of heat waves in Hungary," *Advances in Geosciences*, vol. 35, pp. 115–122, 2013.

[56] M. Kiss, Á. Takács, R. Pogácsás, and Á. Gulyás, "The role of ecosystem services in climate and air quality in urban areas: Evaluating carbon sequestration and air pollution removal by street and park trees in Szeged (Hungary)," *Moravian Geographical Reports*, vol. 23, no. 3, pp. 36–46, 2015.

[57] Á. Takács, M. Kiss, E. Tanács, L. Varga, and Á. Gulyás, "Investigation of tree stands of public spaces in Szeged," *Journal of Environmental Geography*, vol. 8, pp. 33–39, 2015.

[58] Á. Takács, M. Kiss, A. Hof, E. Tanács, Á. Gulyás, and N. Kántor, "Microclimate modification by urban shade trees – an integrated approach to aid ecosystem service based decision-making," *Procedia Environmental Sciences*, vol. 32, pp. 97–109, 2016.

[59] Á. Takács, A. Kovács, M. Kiss, Á. Gulyás, and N. Kántor, "Study on the transmissivity characteristics of urban trees in Szeged, Hungary," *Hungarian Geographical Bulletin*, vol. 65, no. 2, pp. 155–167, 2016.

[60] C. J. Willmott, "On the validation of models," *Physical Geography*, vol. 2, no. 2, pp. 184–194, 1981.

[61] C. J. Willmott, "Some comments on the evaluation of model performance," *Bulletin of the American Meteorological Society*, vol. 63, no. 11, pp. 1309–1313, 1982.

[62] EC European Commission, *Towards an EU Research and Innovation Policy Agenda for Nature-Based Solutions &Amp; Re-Naturing Cities. Final Report of The Horizon 2020 Expert Group on 'Nature-Based Solutions' and Re-Naturing Cities. Directorate-General for Research and Innovation*, Brussels, Belgium, 2015.